Published in final edited form as:
J Phys Chem A. 2012 April 12; 116(14): 3598–3610. doi:10.1021/jp301345h.

Generation of Phosphorescent Triplet States *via* Photoinduced Electron Transfer: Energy and Electron Transfer Dynamics in Pt Porphyrin-Rhodamine B Dyads

Tomoyasu Mani[1], **Dariusz M. Niedzwiedzki**[2], and **Sergei A. Vinogradov**[1,*]

[1]Department of Biochemistry and Biophysics, University of Pennsylvania, Philadelphia, PA 19104 USA

[2]Photosynthetic Antenna Research Center (PARC), Washington University, Saint Louis, MO 63130, USA

Abstract

Control over generation and dynamics of excited electronic states is fundamental to their utilization in all areas of technology. We present the first example of multichromophoric systems in which emissive triplet states are generated *via* a pathway involving photoinduced electron transfer (ET), as opposed to local intrachromophoric processes. In model dyads, PtP-Ph_n-$pRhB^+$ (**1**-**3**, n=1-3), comprising platinum(II) *meso*-tetraarylporphyrin (PtP) and rhodamine B piperazine derivative ($pRhB^+$), linked by oligo-*p*-phenylene bridges (Ph_n), upon selective excitation of $pRhB^+$ at a frequency below that of the lowest allowed transition of PtP, room-temperature $T_1 \rightarrow S_0$ phosphorescence of PtP was observed. The pathway leading to the emissive PtP triplet state includes excitation of $pRhB^+$, ET with formation of the singlet radical pair, intersystem crossing within that pair and subsequent radical recombination. Due to the close proximity of the triplet energy levels of PtP and $pRhB^+$, reversible triplet-triplet (TT) energy transfer between these states was observed in dyads **1** and **2**. As a result, the phosphorescence of PtP was extended in time by the long decay of the $pRhB^+$ triplet. Observation of ET and TT in the same series of molecules enabled direct comparison of the distance attenuation factors β between these two closely related processes.

Keywords

phosphorescence; photoinduced electron transfer; triplet-triplet energy transfer; platinum porphyrins

Introduction

Control over emissivity and dynamics of excited states of molecules is central to practical utilization of these states in all areas of technology and medicine. We are particularly interested in triplet electronic spin states, whose applications encompass medical photodynamic therapy,[1,2] energy up-conversion by triplet-triplet annihilation,[3,4] organic light emitting devices (OLED)[5,6] and biological imaging of oxygen.[7,8] In imaging applications, such as oxygen imaging by phosphorescence lifetime,[9] the ability to impose

*vinograd@mail.med.upenn.edu.

Supporting Information. Quantum yield calculations, absorption and emission spectra, phosphorescence decay curves, measurements at 77K, NSTA data for compounds **2** and **3**, FSTA data for compound **2**, simulations, rate constants table. This material is available free of charge *via* the Internet at http://pubs.acs.org.

control over spatial localization of triplet states of probe molecules, e.g. by way of applying external optical or magnetic fields, may lead to new ways to integrate diffuse phosphorescence lifetime imaging[10,11] with other imaging modalities, thereby enhancing informational content and improving spatial imaging resolution. Similarly, in photodymanic therapy, controlling formation of dark triplet states for generation of singlet oxygen would be invaluable for confining the photodynamic action selectively to the diseased tissue, while reducing undesirable collateral damage. In view of these applications, molecules with intricate energy and electron transfer pathways, providing opportunities for controlling rates and yields of formation of triplet states, are of considerable interest.

Recently we described molecular systems, in which emissive triplet states of Pt(II) porphyrins were populated *via* a route including Förster-type energy transfer from appended multiphoton absorbing antenna chromophores.[12-14] These molecules appeared very useful as probes in two-photon phosphorescence lifetime microscopy (2PLM) of oxygen.[14-16] One studied system comprised Pt(II) tetrabenzoporphyrin (PtTBP) – Rhodamime B (RhB^+) dyad.[13] Upon excitation of RhB^+, fast energy transfer from the RhB^+ singlet state ($^{S1}RhB^+$) onto PtTBP and subsequent intersystem crossing (ISC) yielded local PtTBP triplet (^{T1}PtTBP), which was de-populated *via* efficient $^{T1}PtTBP \rightarrow RhB^+$ electron transfer (ET), followed by non-radiative recovery of the ground state species. (Note that rhodamine B is a cation, and therefore its one-electron reduction leads to the neutral radical).

Analyzing energy and electron flow in *antenna* (A) – triplet *core* (C) dyads we reasoned that if a radical pair state (RP) would have its energy higher than the emissive local triplet state of the core emitter ($^CT_1$), and the corresponding singlet state of the core ($^CS_1$) would lie above the initially excited singlet state of the antenna ($^AS_1$), one likely evolution pathway for the system would be: 1) the ET between the antenna and the core, 2) formation of the singlet radical pair (RP_S), 3) intersystem crossing (RP-ISC) with formation of the triplet RP_T, and 3) subsequent decay of RP_T into $^CT_1$ and $^AS_0$ (Fig. 1). Alternatively, singlet radical pair RP_S would recombine directly with regeneration of the ground state species. One attractive feature of such scheme would be the possibility to tune the rate of the RP-ISC, e.g. by affecting the spin dynamics in the RP *via* modulation of hyperfine interactions,[17] and thereby to impose magnetic control over the formation of the triplet states. On the other hand, the ability to generate an emissive triplet state *via* ET, as opposed to having to deal with ET to prevent unwanted phosphorescence quenching – a problem we encountered in construction of two-photon oxygen probes,[13] – would greatly extend the choice of antenna chromophores suitable for construction of these useful sensors.[18]

Schemes similar to the one shown in Fig. 1 are common for ET systems exhibiting magnetic field effects on the spin dynamics in radical pairs.[17,19-22] Such systems are currently deemed central for biological magneto-sensory mechanisms[23-28] as well as form the basis for several spectroscopic techniques, including Chemically Induced Dynamic Nuclear polarization (or CIDNP)[29,30] and a set of methods collectively known as Optically Detected Magnetic Resonance (ODMR).[31-33] The latter play an important role in studies of natural photosynthetic systems[34-37] and related artificial mimics, which are important for light harvesting, molecular electronics and spintronics applications.[22,24] Not surprisingly, very large number of models with energy layouts resembling that in Fig. 1 has been published to date.[20,22,38] Systems most related to our studies utilize emissive ^{3}MLCT states of $Ru^{2+}(bpy)_3$ or similar complexes usually as *initial* states in ET reactions.[39,40] There are also reports where phosphorescent metalloporphyrins participate in triplet-triplet energy transfer as acceptors.[41,42] However, to the best of our knowledge, molecules in which phosphorescent triplet states are the *final* states in cascades involving ET and RP-ISC have never been disclosed.

In the present paper we report dyads, in which the roles of the antenna and the triplet core are played by RhB^+ and a Pt(II) tetraarylporphyrin (PtP), respectively, whereby the pathway depicted in Fig. 1 allows observation of the PtP phosphorescence without directly exciting PtP. To investigate our model systems we performed optical spectroscopic studies on the microsecond, nanosecond and femtosecond time scales in order to characterize the transient intermediates. One intriguing feature of the reported molecules is existence of a thermal equilibrium between the triplet states of the dyad components (^{T1}RhB and ^{T1}PtP), which is manifested by delayed phosphorescence of PtP, presumably mediated by the triplet-triplet (TT) energy transfer. Although observation of dark triplet states *via* coupled emissive triplet states has been previously reported, [43-46] in our case the presence of both ET and TT in the same series of bichromophoric molecules makes it possible to directly compare distance attenuation factors β between these two closely related processes.

Experimental Methods

General information

All solvents and reagents were obtained from standard commercial sources and used as received. Selecto silica gel (Fisher Scientific, particle size 32-63 micron) was used for column chromatography. ^{1}H NMR spectra were recorded on a Varian Unity 400 MHz spectrometer. Mass-spectra were obtained on a MALDI-TOF MS Microflex LRF instrument (Bruker Daltonics), using α-cyano-4-hydroxycinnamic acid as a matrix. All the photophysical and electrochemical measurements were performed in anhydrous benzonitrile at 22°C, unless otherwise noted.

Optical measurements

UV-vis absorption spectra were recorded on a Perkin-Elmer Lambda 35 UV-Vis spectrophotometer. Steady-state and time-resolved phosphorescence measurements were performed on a FS900 spectrofluorometer (Edinburgh Instruments, UK), equipped with R2658P PMT (Hamamatsu). Time-resolved phosphorescence measurements were performed using either the FS900 instrument with a xenon flash lamp as the excitation source or an in-house constructed time-domain phosphorometer. FS900 allows measurements of emission decays with time constants >20 μs due to its rather long IRF. The custom-built instrument is based on a multichannel data acquisition board (NI-6251 USB, National Instruments), operating at software-selectable digitization frequencies of up to 1.25 MHz. The excitation sources in the instrument are white LEDs (1W Lumiled, Phillips, <10 ns rise time), and the detector is an avalanche photodiode (Hamamatsu). Both the LEDs and the detector were equipped with appropriate optical filters (narrow-band for excitation and long-pass for emission). The light was coupled to the instrument using plastic fibers (3 mm in diameter). The IRF of the phosphorometer has FWHM of ~3 μs, permitting highly accurate measurements of phosphorescence decays with time constants ranging from >3 μs to up to 100 ms. The software for the instrument is written in C/C++ (Qt, Nokia).

Time-resolved fluorescence measurements were performed by the time-correlated single photon counting method (TCSPC). The TCSPC system consisted of a picosecond diode laser (PicoQuant LDH-C-400, λ_{max}=408 nm, FWHM~100 ps, 40 MHz rep. rate), multichannel-plate PMT (Hamamatsu R2809U) and a TCSPC board (Becker & Hickl, SPC-730).

Quartz fluorometric cells (1 cm optical path length) were used in all optical experiments. The samples were deoxygenated by Ar bubbling or by applying four pump-freeze-thaw cycles. Quantum yields were measured against fluorescence of Rhodamine 6G in EtOH (Φ_{fl}=0.94),[47] using rigorously deoxygenates solutions. Time-resolved emission spectra,

obtained using the FS900 instrument, were linearly decomposed into sums of their principle components, i.e. fluorescence of RhB^+ and phosphorescence of PtP, in order to obtain the quantum yields of these emission types individually.

Global fitting was performed using OriginPro 8.5 (OriginLab, MA) and MATLAB R2009a (MathWorks, MA). Decay fitting, spectral deconvolution and maximum entropy analysis were performed using custom written software.[48]

Nanosecond transient absorption spectroscopy (NSTA)

The NS-TA setup consisted of a frequency-doubled Nd:YAG laser as pump (Quanta-Ray DCR-2A, λ_{max}=532 nm, pulse width 10 ns, 10 Hz rep. rate, ~15 mW), a flash lamp (Hamamatsu, pulse width ~2 μs) as a white-light probe source and a monochromator (SPEX) with a diode-array detector (Princeton Instruments, DIDA-512). Light at 532 nm excites both PtP and RhB^+; however, the absorption at this wavelength is strongly dominated by RhB^+ (>90%). Therefore, for the purposes of our analysis it was reasonable to assume that the contributions of pathway(s) resulting from direct excitation of PtP were insignificant. The optical densities of the samples were adjusted to be 0.3-0.5 OD at the excitation wavelength.

Femtosecond transient absorption spectroscopy (FSTA)

Femtosecond time-resolved pump-probe absorption experiments were carried out using a Helios spectrometer (Ultrafast Systems, LCC), coupled to a femtosecond laser system (Spectra-Physics). The system consisted of a Solstice one-box regenerative amplifier, a Mai-Tai Ti:sapphire oscillator as the seeding source and an Empower diode-pumped solid-state pulsed green laser as the pump. The pulse had FWHM ~90 fs at 800 nm with energy of ~3.5 mJ/pulse at 1 kHz repetition rate. The output of the amplifier was divided by a beam splitter. The first beam (ca 90% of the total power) was used as the input for a Topas-C optical parametric amplifier, equipped with a Berek extension (Light Conversion Ltd., Lithuania). The second beam (10% power) was used to generate probe pulses in the Helios spectrometer. The white light continuum pulse in the visible (VIS) region was generated by a 3 mm sapphire plate. The near infra-red (NIR) probe pulse was generated using a proprietary crystalloid plate. A complementary metal-oxide-semiconductor (CMOS) linear array sensor with 1024 pixels was used for detection in the VIS range, while a 256 pixel InGaAs linear diode array was used in the NIR range. To provide isotropic excitation of the sample and to avoid pump-probe polarization effects, the pump beam was depolarized. Individual ΔA (OD) measurements were acquired at a frequency of 500 Hz and averaged over 2 s periods. The energy of the pump beam was set between 2 and 4 μJ/pulse over a spot size of 1 mm in diameter, which corresponds to the energy density of 1×10^{15}-1.5×10^{15} photons/cm^2 per pulse, depending on the excitation wavelength (405-580 nm). The optical densities were adjusted to be 0.8 OD at 560 nm and 0.5 OD at 510 nm (1 cm optical path length) for excitation for RhB^+ and PtP, respectively. During the measurements, the samples were continuously stirred by a magnetic stirrer.

Electrochemical methods

Cyclic voltammetry experiments were performed in an anaerobic glove box using a potentiostat workstation (BAS 100B, Bioanalytical Systems, Inc.) and anhydrous benzonitrile as a solvent. Tetrabutylammomium hexafluoro-phosphate (TBAP) was used as the supporting electrolyte (100 mM). Pt electrode (1.6 mm diameter) was used as the working electrode, an Ag wire as the quasi-reference electrode and a Pt wire as the counter electrode. Ferrocene (Fc) was used as the internal standard; all values are reported relative to Fc^+/Fc couple (scan rate 0.1 V/s). The three electrodes were fitted into a Claisen Adapter (Kontes Glass Company, Vineland, NJ) with working and reference electrodes positioned as

close as possible to minimize the ohmic resistance. At each scan rate, at least five scans were performed to ensure stability of the system.

Synthesis

The complete synthesis is outlined in Scheme 1. All free-base porphyrins were synthesized by the Lindsey method.[49] Platinum was inserted upon refluxing the porphyrins with $PtCl_2$ in anhydrous benzontitrile. Rhodamine B piperazine amide ($pRhB^+$) was synthesized from RhB^+ following the reported procedure.[50] PtP's and $pRhB^+$ were coupled to each other using the HBTU-mediated peptide coupling method. The overall yields of compounds **1**-**3**, starting from the assembly of initial porphyrins, were 4.8%, 5.4% and 0.5%, respectively.

5-(4-methoxycarbonylphenyl)-10,15,20-triphenylporphyrin (H_2P-Ph_1CO_2Me)

A mixture of pyrrole (1.6 g, 24 mmol), benzaldehyde (1.9 g, 18 mmol) and methyl 4-formylbenozate (1.0 g, 6.1 mmol) in CH_2Cl_2 (600 mL) was stirred under Ar for 30 min. $BF_3{\cdot}Et_2O$ (0.61 g, 4.87 mmol) was added in one portion, the mixture was shaded from the ambient light and left under stirring at r.t. for additional 2 hrs. 2,3-Dichloro-5,6-dicyano-1,4-benoquinone (DDQ) (1.38 g, 6.1 mmol) was added, and the mixture was left overnight under stirring. The resulting solution was washed with Na_2SO_3 aq (10 %), $NaCO_3$ aq (10 %), HCl aq (10%), NaOH aq (10 %) and then with distilled water. The organic phase was collected, dried over Na_2SO_4, and the solvent was evaporated to dryness. The residual material was purified by column chromatography on silica gel using CH_2Cl_2/hexane mixture (2:3 by volume) as the mobile phase. The second band was collected, the solvent was evaporated and the remaining solid was dried in vacuum to afford the title compound as a purple solid (230 mg, 5.6 %). The spectroscopic data matched those previously reported.[51]

Pt(II) 5-(4-methoxycarbonylphenyl)-10,15,20-triphenylporphyrin (PtP-Ph_1CO_2Me)

Free-base porphyrin H_2P-Ph_1CO_2Me (60 mg, 0.09 mmol) was dissolved in benzonitrile (10 mL), $PtCl_2$ (47 mg, 0.18 mmol) was added in one portion, and the mixture was set to reflux under Ar. The reaction was stopped when the absorption band near 420 nm (CH_2Cl_2), characteristic of the porphyrin dication, disappeared. Complete conversion into the Pt complex required 6-8 hrs. The solvent was evaporated in vacuum, and the residue was purified by column chromatography on silica gel, using CH_2Cl_2 as the mobile phase, to afford the product as an orange powder (76 mg, 99 %). Spectroscopic data matched those previously reported.[51]

Pt(II) 5-(4-carboxylphenyl)-10,15,20-triphenylporphyrin (PtP-Ph_1CO_2H)

PtP-Ph_1CO_2Me (75 mg. 0.086 mmol) was dissolved in the mixture of THF (50 mL) and EtOH (1 mL). A pellet of KOH was added to the solution, and the mixture was stirred at r.t. for 8 hrs. The solvents were removed under vacuum, and the remaining solids were dissolved in water (ca 20 ml). The solution was filtered, neutralized by HCl, the precipitate was collected by centrifugation, washed with water and dried in vacuum. The title compound was obtained as an orange solid (74 mg, 99 %). ^{1}H NMR (DMSO, δ): 8.71 (br s, 8H, pyrrole-βH), 8.31 (m, 2H, ArH), 8.23 (d, J = 8 Hz, 2H, ArH), 8.14 (m, 6H, *o*-PhH), 7.78 (m, 9H,m,p-PhH); UV-Vis (CH_2Cl_2) λ_{max}: 403, 511, 542 nm; MALDI-TOF (m/z): calcd for $C_{45}H_{28}N_4O_2$: 851.19; found; 851.633.

5-(4-methoxycarbonylbiphenyl)-10,15,20-triphenylporphyrin (H_2P-Ph_2CO_2Me)

H_2P-Ph_2CO_2Me was synthesized in a similar fashion as H_2P-Ph_1CO_2Me, using pyrrole (0.28 g, 4.2 mmol), benzaldehyde (0.33 g, 3.1 mmol) and methyl 4-formyl-4′-methoxycarbonyl-biphenyl (0.25 g, 1.0 mmol) as starting materials. The title compound was obtained as a purple solid (60 mg, 7.7 %). ^{1}H NMR ($CDCl_3$, δ): 8.92 (d, J = 4 Hz, 2H,

pyrrole-βH), 8.87 (m, 6H, pyrrole-βH), 8.61 (m, 2H, ArH), 8.33 (d, J = 8 Hz, 2H, ArH), 8.28 (d, J = 8 Hz, 2H, ArH), 8.24 (m, 4H, ArH), 8.07-7.99 (m, 6H, *o*-PhH), 7.82-7.74 (m, 9H, *m*,*p*-PhH), 4.03 (s, 3H, -$COOCH_3$), −2.74 (s, 2H, −2NH); UV-Vis (CH_2Cl_2) λ_{max}: 420, 516, 551, 591, 648 nm; MALDI-TOF (m/z): calcd for $C_{52}H_{36}N_4O_2$: 748.28; found; 749.469 [M $+H^+$].

Pt(II) 5-(4-methoxycarbonylbiphenyl)-10,15,20-triphenylporphyrin (PtP-Ph_2CO_2Me)

The title compound was synthesized from H_2P-Ph_2CO_2Me (20 mg, 0.027 mmol) in a similar fashion as PtP-Ph_1CO_2Me (see above) The target compound was obtained as an orange powder (20 mg, 80 %). UV-Vis (CH_2Cl_2) λ_{max}: 404, 511, 544. MALDI-TOF (m/z): calcd for $C_{52}H_{34}N_4O_2$: 941.93; found; 942.34 [M+H^+].

Pt(II) 5-(4-carboxybiphenyl)-10,15,20-triphenylporphyrin (PtP-Ph_2CO_2H)

PtP-Ph_2CO_2H was synthesized in a similar fashion as PtP-Ph_1CO_2H (see above) starting from PtP-Ph_2CO_2Me (20 mg, 0.021 mmol). The title compound was obtained as orange solid (19 mg, 96 %). ^{1}H NMR (THF, δ): 10.84, (s, 1H, COOH), 8.83 (d, J = 4 Hz, 2H, pyrrole-βH), 8.75 (d, J = 4 Hz, 2H, pyrrole-βH), 8.74 (br s, 4H, pyrrole-βH), 8.28 (d, J = 8 Hz, 2H, ArH), 8.24 (d, J = 8 Hz, 2H, ArH), 8.17 (m, 6H, *o*-PhH), 8.16 (d, J = 8 Hz, 2H) 8.08 (d, J = 8 Hz, 2H), 7.77 (m, 9H, *m*,*p*-PhH). UV-Vis (CH_2Cl_2) λ_{max}: 403, 513, 544 nm. MALDI-TOF (m/z): calcd for $C_{51}H_{32}N_4O_2$: 927.22; found; 928.45 [M+H^+].

5-(4-bromophenyl)-10,15,20-triphenylporphyrin (H_2P-Br)

H_2P-Br was synthesized as previously reported[52] and isolated as a purple solid (460 mg, 3.1 %). MALDI-TOF (m/z): calcd for $C_{44}H_{29}BrN_4$: 694.16; found; 695.15 [M+H^+].

5-(4-methoxycarbonyl-*p*-triphenyl)-10,15,20-triphenylporphyrin (H_2P-Ph_3CO_2Me)

1) H_2P-Br (40 mg, 0.057 mmol), bis(pinacolato)diboron (37 mg, 0.144 mmol) and KOAc (0.23 g, 0.58 mmol) were dissolved in DMF (1 ml). $PdCl_2(dppf)_2$ (9 mg, 0.012 mmol, 20 %), used as a catalyst in this Miyaura coupling reaction, was dissolved separately in DMF (1 ml). The solution of the catalyst was added to the mixture of the reactants, and it was stirred vigorously at 80°C for 12 hrs. The mixture was cooled down, CH_2Cl_2 10 mL) was added and the resulting solution was washed with water (3×10 mL) in a separatory funnel. The organic phase was collected, dried over Na_2SO_4, and the solvent was evaporated to dryness. The remaining solid was purified by column chromatography on silica gel (CH_2Cl_2/ hexane=1:1) to afford the target porphyrin-pinacolatoboron as a purple solid after removing the solvent and drying the product in vacuum (20 mg, 47 %). MALDI-TOF (m/z): calcd for $C_{50}H_{41}BN_4O_2$: 740.70; found; 741.32 [M+H^+]. The spectroscopic data matched those previously reported.[53]

2) Porphyrin-pinacolatoboron, obtain at the previous step (20 mg, 0.027 mmol), 4-bromo-4′-methoxycarbonyl-biphenyl (12 mg, 0.041 mmol) and Cs_2CO_3 (22 mg, 0.067 mmol) were dissolved in DMF (3 ml). $Pd(PPh_3)_4$ (3 mg, 0.003 mmol, 10 %) used as a catalyst, was dissolved separately in DMF (1 mL). The catalyst solution was added to the mixture of the reactants, and it was stirred vigorously at 80 °C for 12 hrs. The reaction mixture was cooled down, CH_2Cl_2 (10 mL) was added, and the resulting solution was washed with water (3×10 mL). The organic phase was collected, dried over Na_2SO_4 and the solvent was evaporated to dryness. The remaining solid was purified by column chromatography on silica gel using CH_2Cl_2 as the mobile phase. The title compound was isolated as a purple solid (12 mg, 55 %). ^{1}H NMR ($CDCl_3$, δ): 8.95 (d, J = 4 Hz, 2H, pyrrole-βH), 8.88 (m, 6H, pyrrole-βH), 8.33 (d, J = 8 Hz, 2H), 8.24 (m, 6H, *o*-PhH), 8.20 (d, J = 8 Hz, 2H, ArH), 7.88 (d, J = 8 Hz, 2H, ArH), 7.82 (d, J = 8 Hz, 2H, ArH), 7.79 (m, 9H, *m*,*p*-PhH), 7.49 (m, 4H, ArH), 4.0 (s, 3H, -

$COOCH_3$), −2.73 (s, 2H, −2NH). UV-Vis (CH_2Cl_2) λ_{max}: 421, 516, 550, 595, 649 nm. MALDI-TOF (m/z): calcd for $C_{58}H_{40}N_4O_2$: 824.96; found; 825.33 [$M+H^+$].

Pt(II) 5-(4-carboxy-*p*-triphenyl)-10,15,20-triphenylporphyrin (PtP-Ph_3CO_2H)

H_2P-Ph_3CO_2H (12 mg, 0.14 mmol) was dissolved in benzonitrile (60 mL), $PtCl_2$ (22 mg, 0.060 mmol) was added, and the mixture was set to reflux under Ar. The reaction was stopped when the absorption band of the porphyrin dication disappeared. Complete conversion to the Pt complex required ca 12 hrs. The solvent was evaporated in vacuum, and the residue was purified by column chromatography (silica gel, CH_2Cl_2) to afford the Pt complex as an orange powder. The obtained Pt complex was dissolved in THF (10 mL). MeOH (0.5 mL) and a pellet of KOH were added, and the mixture was left under stirring at r.t. for 12 hrs. The solvents were removed under vacuum, and the water was added. The solution was filtered and neutralized by addition of HCl. The precipitate was collected by centrifugation, washed with water and dried in vacuum. The title compound was obtained as orange solid (2.0 mg, 14 %). UV-Vis (CH_2Cl_2) λ_{max}: 403, 512, 542 nm. MALDI-TOF (m/z): calcd for $C_{57}H_{36}N_4O_2Pt$: 1004.00; found; 1004.80 [$M+H^+$].

PtP-Ph_1-pRhB$^+$ (1)

PtP-Ph_1CO_2H was dissolved in DMF (20 mL) and stirred under Ar for 5 min. Diisopropylethylamine (DIPEA; 36 mg, 0.28 mmol) and o-benzotriazole-N,N,N′N′-tetramethyl-uronium-hexafluoro-phosphate (HBTU; 11 mg, 0.029 mmol) were added to the mixture in one portion, and it was stirred under Ar for another 5 min. pRhB$^+$ (15 mg, 0.029 mmol) was added, and the mixture was left under stirring and Ar for 24 hrs. The solvent was removed under vacuum, and the residue was purified by column chromatography (silica gel, THF). The second band was collected, the solvent was evaporated, and the product was dried in vacuum. The title compound was isolated as a purple solid (25 mg, 81 %). ^{1}H NMR (DMSO, δ): 8.77 (d, J = 4 Hz, 2H), 8.71 (m, 6H), 8.22 (m, 2H), 8.14 (m, 6H), 8.07 (d, J = 8 Hz, 2H), 8.04 (br s, 1H), 8.00 (d, J = 8 Hz, 2H), 7.91 (br s, 1H), 7.89 (br s, 1H), 7.78 (m, 9H), 7.55 (d, J = 8 Hz, 2H), 7.11 (m, 2H), 6.94 (d, J = 2 Hz, 2H), 3.64 (q, J = 8 Hz, 8H), 2.85 (br s, 4H), 2.69 (br s, 4H), 1.32-1.28 (m, 12H); UV-Vis (PhCN) λ_{max} (log ε): 405 (5.2 ± 0.1), 513 (4.4 ± 0.1), 566 (4.80 ± 0.1) nm; MALDI-TOF (m/z): calcd for $C_{77}H_{65}N_8O_3Pt^+$: 1344.48; found; 1344.55.

PtP-Ph_2-pRhB$^+$ (2)

The title compound was synthesized in a similar fashion as **1** (see above) from PtP-Ph_2CO_2H (20 mg, 0.021 mmol) and pRhB$^+$ (14 mg, 0.027 mmol) as starting materials. **2** was isolated as a purple solid (28 mg, 92 %). ^{1}H NMR (DMSO, δ): 8.82 (d, J = 4 Hz, 2H), 8.75 (d, J = 4 Hz, 2H), 8.72 (br s, 4H), 8.30 (m, 4H), 8.23 (d, J = 8 Hz, 2H), 8.14 (m, 6H), 7.81 (m, 9H), 7.71 (d, J = 8 Hz, 2H), 7.42 (br s, 1H), 7.40 (br s, 1H), 7.20 (d, J = 4 Hz, 2H), 7.17 (d, J = 4 Hz, 2H), 7.05 (br s, 1H), 6.78 (m, 2H), 3.64 (q, J = 8 Hz, 8H), 3.46 (m, 4H), 3.20 (m, 4H), 1.32-1.28 (m, 12H); UV-Vis (PhCN) λ_{max} (log ε): 405 (5.2 ± 0.1), 514 (4.4 ± 0.1), 566 (4.8 ± 0.1) nm; MALDI-TOF (m/z): calcd for $C_{83}H_{69}N_8O_3Pt^+$: 1421.52; found; 1421.61.

PtP-Ph_3-pRhB$^+$ (3)

The title compound was synthesized in a similar fashion **1** by using PtP-Ph_3CO_2H (2 mg, 0.002 mmol) and pRhB$^+$ (1.2 mg, 0.003 mmol) as starting materials. **3** was isolated as a purple solid (2 mg, 65 %). ^{1}H NMR (DMSO, δ): 8.81 (d, J = 4 Hz, 2H), 8.71 (m, 6H), 8.26 (d, J = 4 Hz, 2H), 8.14 (m, 6H), 8.11 (d, J = 8 Hz, 2H), 7.92 (d, J = 8 Hz, 2H), 7.86 (d, J = 8 Hz, 2H), 7.80 (m, 9H), 7.73 (br s, 3H), 7.49 (m, 4H), 7.10 (m, 2H), 6.94 (m, 2H), 6.83 (br s, 2H), 3.63 (m, 8H), 3.56 (t, J = 4 Hz, 4H), 3.20 (m, 4H), 1.23-1.18 (m, 12H); UV-Vis

(PhCN) λ_{max} (log ε): 405 (5.2 ± 0.1), 515 (4.5 ± 0.1), 567 (5.0 ± 0.1) nm; MALDI-TOF (m/z): calcd for $C_{89}H_{73}N_8O_3Pt^+$: 1497.66; found; 1498.32.

Results and Discussion

Choice of chromophores

The chromophores suitable for the proposed above scheme must satisfy several energetic requirements (Fig. 1). First of all, the initially populated excited singlet state of the antenna ($^AS_1$) must have its energy higher than the energy of the triplet state of the core ($^CT_1$). At the same time, $^AS_1$ must lie below the singlet state of the core ($^CS_1$) in order to prevent population of $^CS_1$ either directly or *via* $^AS_1 \rightarrow {}^CS_1$ energy transfer(s), competing with ET. Secondly, the energy of the radical pair state RP, created as a result of the ET, must be higher than that of $^CT_1$ to allow downhill radical recombination R_T. These two requirements set the limits for the entire energy cascade, which has to fit within the singlet-triplet gap (2J) of the phosphorescent core.

Based on our previous spectroscopic and electrochemical investigations of Pt porphyrins,[18] we conjectured that a suitable dyad could be constructed from Rhodamine B (RhB^+) and a PtP (Pt(II) tetraarylporphyrin) with appropriately tuned oxidation potential. From the synthetic point of view, tetraarylporphyrins with various substitution patterns can be conveniently generated using well-established synthetic protocols.[49,54] A piperazine amide derivative of RhB^+, $pRhB^+$, directly suitable for amide coupling reactions, is accessible *via* a simple and reliable method.[50]

In Pt porphyrins strong spin-orbit coupling is responsible for high rates of both $S_1 \rightarrow T_1$ intersystem crossing and subsequent radiative $T_1 \rightarrow S_0$ decay,[55] thereby causing bright phosphorescence.[56] Peripheral substituents in the *meso*-aryl rings practically do not affect spectroscopic features of PtP's, while significantly altering their electrochemical potentials.[18] This feature gives the desired flexibility of tuning the level of the RP state without affecting the rest of the chromophoric system.

The lowest energy Q_{00} state of a representative PtP, Pt tetraphenylporphyrin (PtTPP) (λ_{max}~541 nm, 2.29 eV), is located above the $pRhB^+$ transition (λ_{max}~567 nm, 2.19 eV). In fact, the $pRhB^+$ absorption band extends beyond 600 nm, so it is possible to excite $pRhB^+$ selectively without directly populating the Q_{00} state (^{S1}PtP) using wavelengths in the range of ~560-600 nm. The energy of the PtP triplet state, based on its phosphorescence maximum (λ_{max} =670 nm, 1.85 eV for PtTPP), is below that of $^{S1}pRhB^+$ state. The entire 2J gap of PtP is ca 0.44 eV.

In PtP-$pRhB^+$ pairs, $^{S1}pRhB^+$ (λ_{ex}= 585 nm, 2.12 eV) is expected to play the role of the electron acceptor, although the exact energy of the RP state depends on the substituents in the porphyirn macrocycle. For PtTPP and $pRhB^+$, whose ground state oxidation and reduction potentials in DMF are +1.16V *vs* SCE ($PtTPP^+$/PtTPP) and −0.85V vs SCE ($pRhB^+$/pRhB), respectively,[18,57] the ET driving force ΔG=−0.11 eV is expected in accordance with the Rehm-Weller equation.[58] Thus, the energy of the radical pair (ca 2.0 eV) is expected be ca 0.15 eV higher than the energy of ^{T1}PtP.

Based on these considerations, we chose to study bichromophoric assemblies comprising PtTPP derivative (from here and throughout the text we refer to Pt porphyrin components of the studied dyads simply as PtP), and $pRhB^+$ connected by oligo-*p*-phenylene linkers (Chart 1, Ph_n, n=1-3: compounds **1**-**3**) and an amide bond. Oligo-*p*-phenylenes have been extensively used as bridges in ET models,[59] as they can be conveniently constructed using

Suzuki-Miyaura chemistry.[60] By varying the number of the phenylene fragments in the bridge, distance dependencies of ET and TT processes can be elucidated.

Steady-state spectroscopy

The steady-state absorption and phosphorescence spectra of **1** are shown in Fig. 2A (see Fig. S1-S2 for the spectra of **2** and **3**).

The absorption spectra of compounds **1**-**3** are nearly superpositions of the spectra of the individual chromophores, indicating negligible electronic interactions between PtP and $pRhB^+$ in their ground and excited electronic states. The emission of spectra of **1** (Fig. 2B-D, λ_{ex}=425, 510, 580 nm), as well as of **2** and **3** (Fig. S2), change with excitation wavelength. Assuming that the overall emission is a linear combination of the $pRhB^+$ fluorescence and PtP phosphorescence, we could decompose the spectra into the sums of their components and estimate the corresponding quantum yields (Table 1) (see SI, S2 for details of decomposition and analysis). The fluorescence quantum yield of $pRhB^+$ alone in PhCN was found to be 0.44 (λ_{ex}=510 nm), which is slightly lower than reported for the anionic form of RhB^+ in EtOH (0.65),[47] but higher than that for $pRhB^+$ in EtOH (0.24).[50] The quantum yields of $pRhB^+$ fluorescence in the dyads were found to be 0.19, 0.26, and 0.38 for **1**-**3**, respectively (λ_{ex}=510 nm, ~40% of absorption is due to $pRhB^+$), indicating the presence of additional quenching pathways for the $pRhB^+$ singlet state.

The key feature of the dyads **1**-**3** is that the phosphorescence of PtP could be observed upon excitation of $pRhB^+$ at the frequency below that of the lowest allowed transition of PtP, i.e. λ_{ex}=580 nm. It was manifested by the long-lived decay of phosphorescence upon excitation at 580 nm (Fig. 2E), the identity of which was confirmed by the time resolved spectral data (Fig. 2F). The quantum yield of the phosphorescence observed *via* this pathway was not high (Φ_{phos}~0.001), but the emission was clearly observable, whereas for the reference porphyrins PtP-$Ph_n CO_2H$ (Scheme 1; abbreviated in Table 1 and further in the text as PtP_n) as well as for PtTPP no signal could be detected at all upon excitation in the range of 550-600 nm. Additional arguments speaking against direct excitation of PtP in the dyads include virtually zero molar extinction at 580 nm for all our models, very low excitation intensities employed and, as we show below, the presence of a rise phase in the dynamics of the PtP triplet state with the time constant 100-1000 times lower than that of the direct $S_1 \rightarrow T_1$ ISC within PtP. Therefore, a different pathway exists in the dyads, which originates in the antenna singlet state $^{S1}pRhB^+$ and populates the emissive triplet states of the core PtP's.

Phosphorescence quantum yields of the dyads were measured upon excitation near the Q band maximum (λ_{ex}=510 nm, ~60% of absorption is due to PtP) and found to be lower than those of the corresponding reference porphyrins PtP_n and of PtTPP. Notably, in the series of the reference compounds (PtP_n) the phosphorescence quantum yields decrease with an increase in the length of the oligo-phenylene linker. But in addition, quenching of the PtP triplet states in the dyads appears to be enhanced by the presence of the $pRhB^+$ fragment. This effect could be a combined result of several phenomena. However, one can probably rule out direct quenching of the porphyrin singlet Soret (S_2) or Q (S_1) states by either energy or electron transfer onto $pRhB^+$, since both $S_2 \rightarrow S_1$ internal conversion and $S_1 \rightarrow T_1$ ISC in Pt porphyrins occur on the femotosecond time scale.[61,62] Competing with such fast processes would be improbable. More likely is that the PtP triplet state already after being formed is partially quenched by the TT energy transfer onto $pRhB^+$ (ΔG~−0.05 eV – see below), or by the ET onto $pRhB^+$, even though the latter process is expected to be endergonic. The evidence for the former pathway was indeed obtained by nanosecond pump-probe and time-resolved phosphorescence measurements (see below).

Electron transfer

The most plausible pathway leading to the formation of the triplet state ^{T1}PtP upon population of ^{S1}RhB$^+$ involves ET. Energy transfer processes are much less likely. Indeed, spin-allowed singlet-singlet energy transfer from ^{S1}RhB$^+$ to populate ^{S1}PtP is up-hill ($\Delta E_{00}(^{S1}pRhB^+)$=2.12 eV and $\Delta E_{00}(^{S1}PtP)$=2.3 eV), while the direct singlet-triplet energy transfer ^{S1}RhB$^+ \rightarrow ^{T1}$PtP is spin-forbidden. Another potential pathway could involve ^{S1}RhB$^+ \rightarrow ^{T1}$RhB$^+$ intersystem crossing within pRhB$^+$ itself, followed by the population of the ^{T1}PtP state *via* triplet-triplet (TT) energy transfer. This pathway could be operational in view of the existence of the reversible TT transfer between PtP and pRhB$^+$ (see below). However, transient absorption measurements ruled out this possibility (see below), showing that the ^{T1}PtP state precedes the ^{T1}RhB$^+$ state and not *vice versa*.

On the other hand, the radical pair state, [PtP$^{\bullet+}$-Ph$_n$-pRhB$^{\bullet 0}$], is located down-hill from the initially populated state ^{S1}pRhB$^+$. The Gibbs free energy of the ET (ΔG_{ET}) was estimated to be −0.12 eV using the Rehm-Weller formula: $\Delta G_{ET}=E_{ox}(D)-E_{red}(A)-\Delta E_{00}+\Delta w$,[58] where $E_{ox}(D)$ and $E_{red}(A)$ are the oxidation and reduction potentials of the donor and acceptor, respectively, ΔE_{00} is the excitation energy of the initially populated state and Δw is the electrostatic work term, which in our case is zero, since the ET leads to simple shifting of the charge. The oxidation and reduction potentials of the dyads, measured in benzonitrile solutions, were found to be close for all the compounds **1**-**3**: E_{ox}=+0.53±0.01 V and E_{red}= −1.46±0.03 V; and similar values were obtained for the individual chromophores, E_{ox} for PtP$^+$/PtP and E_{red} for pRhB$^+$/pRhB. Based on these measurements, the energy of the RP state (~2.0 eV), was estimated to be between the energies of ^{S1}pRhB$^+$ (ΔE=2.12 eV) and ^{T1}PtP (ΔE=1.85 eV).

Assuming that the ET in the dyads is the only deactivation pathway for ^{S1}pRhB$^+$ in addition to its natural radiative and non-radiative decays, the ET rate constants (k_{ET}) could be calculated directly from the fluorescence lifetime data (τ_{fl}, Table 1): $k_{ET}=k_{fl}-k_{fl}^0$, where k_{fl} and k_{fl}^0 are the rate constants ($1/\tau_{fl}$) of the fluorescence of pRhB$^+$ in dyads and of free pRhB$^+$, respectively. (Here we assume that the native radiative (k_r) and non-radiative (k_{nr}) decay rate constants ($k_{fl}^0=k_r+k_{nr}$) do not change upon inclusion of pRhB$^+$ into dyads). The k_{ET} values were found to be 6.4×10^8 s^{-1} for **1**, 2.3×10^8 s^{-1} for **2** and 9.7×10^7 s^{-1} for **3**. The rate constant of the fluorescence decay of free pRhB$^+$ is 3.4×10^8 s^{-1}. The rate of the ET is higher than the rate of the pRhB$^+$ fluorescence in dyad **1** and lower than that in dyads **2** and **3**.

Evolution of the radical pair state

Transient electronic absorption spectroscopy allows detection of non-emissive short-lived intermediates in photoinduced ET reactions. We performed femtosecond transient absorption (FSTA) measurements on dyads **1** and **2** in order to capture the spectroscopic signatures and record time evolution of the RP state. In the case of compound **3**, due to the low rate of the ET and consequently a small amount of the RP species formed, observation of the transient spectra was hampered by noise. However, other spectroscopic data (see below) strongly suggest that the dyad **3** undergoes the same pathway as **1** and **2**.

The FSTA spectra of compound **1** upon pulsed excitation at λ_{max}=580 nm (FWHM 90 fs) are shown in Fig. 3A,B (see Fig. S3 for the corresponding spectra of **2**). Global fitting of the transients produced two overlapping but distinct spectral features in the region of 400-520 nm (Fig. 3C; the related decays are shown in Fig. 3D). Based on the comparison with other transients in the spectra and with the literature data, the broad feature decaying with time constant of 540 ps was assigned to the $S_1 \rightarrow S_n$ absorption of pRhB$^+$. This kinetic is similar to the one of the pRhB$^+$ stimulated emission (e.g. at 600 nm), 490 ps, although accuracy in

determination of the latter time constant suffered from the proximity of the laser spectrum. In the near infrared (NIR) region, excited state absorption of $pRhB^+$ is manifested by a broad peak with the maximum near 960 nm, decaying at the matching rate. Notably, the decay times for $^{S1}pRhB^+$ in the dyads and $pRhB^+$ alone obtained by FSTA were shorter than determined by the TCSPC fluorescence lifetime measurements (Table S1). We think that the discrepancy is due to the difference in sampling by the two methods, combined with not perfectly single-exponential nature of the $pRhB^+$ decay. Decay binning in our TCSPC system starts at 600 ps and continues up to 50 ns, therefore weighting towards the long-lived components of the decay. In the FSTA system, the first spectrum is acquired at ~1 ps, and the entire window is 8 ns, amplifying the contribution of the short-lived components.

Interpretation of transient spectra of dyads **1**-**3** was complicated by strongly overlapping absorption bands of multiple participating species, i.e. ground and excited singlet, triplet and radical states of the chromophores. Nevertheless, the peaks at 490 nm and 810 nm could be confidently assigned to the RP state based on the global analysis and spectroelectrochemical data (see below). Remarkably, both peaks rise with the time constant of 420-430 ps ($\sim 2.35\times10^9\ s^{-1}$), which is faster than the decay of the parent state $^{S1}pRhB^+$ ($k_{fl}(\mathbf{1})=10^9\ s^{-1}$). This seemingly paradoxical result, however, can be expected for a two-component system A/B, where both A and B decay with their own rates constants k_A and k_B, and B forms directly from A: A→B. In such a system, if $k_B>k_A$, then observing the evolution of B one would see it rise with the rate k_B, which is actually the rate of its decay, and decay at the rate k_A, which is the decay rate of its precursor (see SI for kinetic equations). Applied to our case, the rate of the formation of RP from $^{S1}RhB^+$ is apparently lower than the rate of the subsequent decay, so that the time constant of the rise (420-430 ps) actually corresponds to the decay of the RP. The fact that we did not observe the decay of the absorption at 490 nm with the time constant corresponding to the decay of $^{S1}RhB^+$ (Fig. 3D) suggests that the long-lived species formed from the RP has its own absorption at the same wavelength and approximately the same molar extinction coefficient. This species is the PtP local triplet state (see below).

Spectroelectrochemical data support our assignment of the RP spectra. Although the absorption spectrum of $pRhB^{0\bullet}$ is not known, the spectrum of the neutral radical of RhB ($RhB^{0\bullet}$) has been reported to have an absorption band near 430 nm.[63] The neutral radical of rhodamine B ethyl ester, known as rhodamine 3B, also has been reported,[64] and it also absorbs around 430-450 nm. PtTPP cation radical ($PtTPP^{+\bullet}$) exhibits a broad absorption band around 600 nm,[57] and in addition has broad absorption centered around 400 nm. In addition to the absorption in the visible range, we also observed a transient peak near 810 nm, partially overlapping with $T_1\rightarrow T_n$ absorption of PtP (broad feature neat 860 nm) (see Fig. S5 and S6 for details). The peak at 810 nm rises with the time constant of 430 ps, close to that of the peak near 490 nm, and tentatively it has been assigned to the RP as well. Additional evidence for the formation of the RP is provided by the negative peak near 510 nm in the decay-associated spectra (Fig. 3C), which is likely to be due to the ground state bleaching of the porphyrin Q-band.

Both nanosecond transient absorption (NSTA) and emission measurements (see below) confirm that upon population of $^{S1}RhB^+$, the dyads eventually evolve with formation of the local triplet state on PtP. It is, therefore, necessary to consider all plausible evolution pathways of the RP, leading to that state (see Fig. 6 for pathway identification). These pathways include: (a) RP-ISC ($^S[PtP^{+\bullet}\text{-}Ph_n\text{-}pRhB^{0\bullet}]\rightarrow{}^T[PtP^{+\bullet}\text{-}Ph_n\text{-}pRhB^{0\bullet}]$), followed by the radical recombination to yield $^{T1}PtP\text{-}Ph_n\text{-}pRhB^+$; (b) RP-ISC, followed by the recombination with formation of the triplet state of $pRhB^+$, $PtP\text{-}Ph_n\text{-}^{T1}pRhB^+$, and subsequent TT energy transfer $PtP\text{-}Ph_n\text{-}^{T1}pRhB^+\rightarrow{}^{T1}PtP\text{-}Ph_n\text{-}pRhB^+$; and (c) the direct transition $^S[PtP^{+\bullet}\text{-}Ph_n\text{-}pRhB^{0\bullet}]\rightarrow{}^{T1}PtP\text{-}Ph_n\text{-}pRhB^+$. Both pathways (a) and (b) proceed *via*

RP-ISC, and, according to our data, pathway (a) appears to be dominant (see below). The rate of the spin-forbidden pathway (c), known as spin-orbit-induced intersystem crossing (SO-ISC),[35] is highly dependent on the mutual orientation of the participating molecular orbitals of the ET partners.[65,66] Molecular dynamics simulations (see Fig. S7) revealed that our dyads exhibit substantial degree of conformational freedom, which is due to rotations around the amide bonds. Conformational flexibility results in a broad distribution of angles between the orbitals of PtP and $pRhB^+$, so that the fraction of time spent by the chromophores in the conformation required for the SO-ISC to occur is probably very small. Therefore, pathway (c) is unlikely to contribute significantly to the evolution of the RP. The other two pathways, (a) and (b), are the key to the formation the local triplet states ^{T1}PtP and ^{T1}RhB.

Local triplet states and triplet-triplet (TT) energy transfer

To investigate the dynamics of the local triplet states in the dyads we performed NSTA and time-resolved phosphorescence measurements. Upon excitation into the red edge of the $pRhB^+$ band (580 nm), **1** and **2** exhibit multiexponential phosphorescence decays in deoxygenated benzonitrile solutions. Almost identical decays were observed when dyads **1** and **2** were excited directly at the PtP Q-band maxima (510 nm). The decays were analyzed by the maximum entropy method (MEM),[48,67] which, in the case of **1**, as an example, revealed a distribution of lifetimes with peaks near τ_{max}~5 μs and τ_{max}~250 μs. The peak near 5 μs was broad and extended towards longer lifetimes, exhibiting decays with lifetimes reaching as high as 70-80 μs. Notably, the precursor porphyrins (PtP_n) and PtTPP under the same conditions reveal narrow unimodal lifetime distributions, corresponding to regular single-exponential kinetics. The decay of **3** was also analyzed by conventional single-exponential analysis (Fig. S8), as this model was sufficient for its phosphorescence kinetics (see below).

Representative NSTA spectra (λ_{ex}=532 nm) for compound **1** are shown in Fig. 4 with the earliest time point of 50 ns (see Fig. S9 for the corresponding spectra of **2** and **3**). Unfortunately, the time period between the last point of the FSTA measurements (7 ns) and the beginning of acquisition of the NSTA data (50 ns) could not be accessed spectroscopically.

The two main features in the NSTA spectra are the $T_1 \rightarrow T_n$ absorption of PtP (positive peak near 455 nm)[55] and the ground state bleaching (GSB) of $pRhB^+$ (negative peak with λ_{max}=567 nm). Importantly, the latter shows a fast decay (τ_d~5 μs), corresponding to the depletion of the $pRhB^+$ ground state, followed by a slow rise (τ_r=200-250 μs), i.e. ground state recovery (Fig. 4B). This long rise was attributed to the $T_1 \rightarrow S_0$ ISC of $pRhB^+$. Indeed, long-lived triplet decay of the parent Rhodamine molecule has been observed previously, also by way of NSTA, in a pyrene-Rh dyad.[68]

In synchrony with fast decaying initial phase of $pRhB^+$ GSB (Fig. 4B, 567 nm trace), PtP triplet-triplet absorption (455 nm trace) is also displaying a fast decaying component. The lifetime distribution of the phosphorescence lifetimes consistently contains significant fraction of decay components near 3-4 μs. These data led us to postulate the existence of the TT energy transfer between ^{T1}PtP and $^{T1}pRhB^+$ states. The directionality of the TT, i.e. from ^{T1}PtP to $^{T1}pRhB^+$, suggests that after the initial electron transfer the RP state undergoes RP-ISC and recombines to yield the local triplet state $^{T1}PtP\text{-}Ph_n\text{-}pRhB^+$, rather than $PtP\text{-}Ph_n\text{-}^{T1}pRhB^+$. Notably, these data also confirm of our central hypothesis, i.e. that the population of the ^{T1}PtP occurs *via* the RP route, as opposed to direct $^{S1}pRhB \rightarrow ^{T1}pRhB$ ISC within the pRhB moiety, followed by TT transfer from $pRhB^+$ to PtP. If the latter was true, the initial phase in the ^{T1}PtP dynamics would be a rise and not decay.

Remarkably, the GSB recovery phase of $pRhB^+$ in **1** and **2** is paralleled by the long-lived components in the PtP phosphorescence (Table 1). These lifetimes are much longer than the native decay of the PtP_n triplet state (τ~30-40 μs), suggesting that it is the slow $^{T1}pRhB^+$ decay that is reflected in the emission of PtP by way of "delayed phosphorescence". Thus, after being populated the $^{T1}pRhB^+$ state either decays to the ground state or undergoes back TT transfer with regeneration of emissive state ^{T1}PtP. Apparently, equilibrium is established between these two states, forming a pool of triplet excitons. The existence of the equilibrium is supported by the fact that the energy of $^{T1}RhB^+$ (1.80-1.84 eV)[69-71] is almost equal to that of ^{T1}PtP (1.85 eV), and the energetics of $^{T1}pRhB^+ \rightarrow {}^{T1}PtP$ process is not completely unfavorable. Furthermore, phosphorescence measurements at 77K (Fig. S11) reveal that the decay of the ^{T1}PtP state in e.g. dyad **1** becomes nearly perfectly single-exponential, having the lifetime (~90 μs) slightly lower that of PtP alone (~120 μs). Hence, at low temperature forward TT transfer becomes slow and only slightly shortens the native PtP decay, while the backward TT transfer virtually stops. In contrast, at high temperature the long-lived non-emissive $pRhB^+$ triplet state is able to act as an "energy reservoir",[72] lengthening the overall lifetime of the phosphorescence, although some energy is inevitably lost *via* the non-radiative $^{T1}pRhB^+$ decay. Similar cases of triplet lifetime lengthening *via* reversible energy transfer have been noted previously.[46,73] Our results highlight the possibility of using multiple isoenergetic triplet states to elongate the lifetime of a triplet exciton, tuning in it in accordance with demands of applications.

One interesting feature of the phosphorescence in dyad **1** is the presence of an extra peak with λ_{max}=720 nm (associated decay time constant 72 μs) that could be clearly observed in the time-resolved phosphorescence spectra of **1** (Fig. 5). Because of its relatively small overall intensity, this peak could not be seen in the steady-state emission spectra, and its unique time signature blended into the lifetime distribution underlying the phosphorescence decay. Compounds **2** and **3** did not show this spectral feature at all. The emission of **1** at 720 nm was quenched by molecular oxygen, as was the PtP phosphorescence, and remained present in solvents of different polarity, such as THF (ε=7.5), benzonitrile (ε=25.0) and DMA (ε=37.8). Based on the combination of these characteristics this spectral band was attributed to the intramolecular triplet exciplex between PtP and $pRhB^+$.

Our assignment was based on exclusion of other potential emitters, such as triplet state of $pRhB,^+$ monomer or ground state dimer, or $pRhB^+$-$pRhB^+$ triplet excimer. The monomer of RhB^+ emits phosphorescence at 690 nm and its phosphorescence is detectable only at low temperature (e.g. 77 K in EtOH/H_2O or EtOH/MeOH),[71,74] The RhB^+ dimer does have an emission peak at 720 nm, but its observation also requires low temperature. Furthermore, the dimer has significantly different absorption spectra,[71] while in our system the absorption of $pRhB^+$ clearly matched that of the RhB^+ monomer. On the other hand, intermolecular $pRhB^+$-$pRhB^+$ triplet excimer, which would have the same emission features as the triplet formed upon excitation of the ground state dimer, could be excluded because sample dilutions had no effect at the emission at 720 nm. The remaining candidate was intramolecular exciplex PtP-$pRhB^+$, which presumably could form directly from the triplet RP. In dyads **2** and **3** similar exciplexes could not form due to considerably longer interchromophoric distances. Based on the steady state and emission spectra, the contribution of the exciplex to the overall energy pathway was minimal.

Energy and electron transfer dynamics

The complete diagram describing the energy and electron transfer pathways in the studied dyads is shown in Fig. 7. The corresponding rate constants are summarized in Table 2.

The dominant pathway occurring in the dyads upon selective excitation of $pRhB^+$ is the following: PtP-Ph_n-$^{S1}pRhB^+ \rightarrow {}^{S}[PtP^{+\bullet}\text{-}Ph_n\text{-}pRhB^{0\bullet}]$ $({}^{S}RP) \rightarrow {}^{T}[PtP^{+\bullet}\text{-}Ph_n\text{-}pRhB^{0\bullet}]$

(^{T}RP)→ ^{T1}PtP-Ph$_n$-pRhB$^+$→ PtP-Ph$_n$-pRhB$^+$ (ground state). TT energy transfer from ^{T1}PtP to ^{T1}RhB plays an important role in elongating the lifetime of the resulting phosphorescence emission, although the intersystem crossing to the ground state of pRhB$^+$ ($k_{isc}^{pRhB^+}$) provides an extra escape passage for the excitation energy. The main competing pathway to the phosphorescence in the dyads is the singlet radical recombination. Its rate (k_{RS}) was not assessed directly, but it is presumed to be comparable to the rate of the triplet recombination times the rate of RP-ISC ($k_{RP\text{-}ISC}\times k_{RT}$), since the phosphorescence quantum yields in the dyads are lower than that of the parent porphyrins. Further work on optimization of such emissive triplet systems will need to focus on minimization of this alternative pathway.

Distance attenuation factors

The dyads prepared in this study are unique in that they feature both ET and TT energy transfer processes. This property is interesting in view of the relationship between the corresponding distance attenuation factors, β^{ET} and β^{TT}, which has been debated in the literature. Closs et al. have originally suggested that the attenuation factor for TT energy transfer (β^{TT}), either *via* direct "through-space" exchange or through saturated bridges, should be two times higher than that for ET. Their TT vs ET studies were based on systems with similar, but not identical donor (D) and acceptor (A) chromophores.[75,76] The theoretical interpretation relied on a simple fact that the Dexter-type TT exchange can be viewed as a concerted transition of one electron and one hole, moving in the same direction. The electron travels from the donor LUMO to the acceptor LUMO, while the hole travels from donor HOMO to the acceptor HOMO. The two transitions are represented by their own electronic coupling matrix elements V_{ET} and V_{HT}, for ET and hole transfer (HT), respectively, which are considered to exhibit very close distance attenuation factors ($\beta^{ET}\approx\beta^{HT}$). Therefore, the coupling matrix element for the TT transfer (V_{TT}) is approximated by the product of the two: $V_{TT}\approx|V_{ET}||V_{HT}|=C\times\exp(-2\beta^{ET} R_{DA})$, where C is a system specific constant, and R_{DA} is the donor-acceptor distance. It follows then that: $\beta^{TT}/\beta^{ET}=2$.

However, later Welter et al. analyzed the data for various D-B-A systems with *p*-phenylene bridges and pointed out that β^{TT} values for bridge-mediated TT energy transfer reactions are not so different from the corresponding β^{ET} values.[77] Still, the data analyzed were obtained using systems featuring not identical chromophore pairs. In this regard, our dyads exhibit ET and TT processes separated in time, but occurring in exactly the same molecules, thus providing opportunity for the direct comparison between β^{ET} and β^{TT}.

The distance dependencies of the ET and TT transfer rate constants for dyads **1**-**3** are shown in Fig. 7A. Their absolute values are different by ~3 orders of magnitude, presumably owing to the difference between the corresponding driving forces, i.e. $\Delta G_{ET}=-0.12$ eV and $\Delta G_{TT}<-0.05$ eV.

In non-adiabatic high temperature regime, the ET rate constant has exponential dependence on the donor-acceptor distance, i.e. $k_{ET}\sim\exp(-\beta^{ET}R_{DA})$.[75,76] Considering that the average distances R_{DA} in our dyads (i.e. interchromophoric edge-to-edge distances) are 13.2 Å and 17.2 Å and 21.2 Å for **1**-**3**, respectively, the attenuation factor β^{ET} for the initial forward electron transfer (k_{ET} in Fig. 6) was determined to be 0.23 Å^{-1}. Notably, β^{ET} values for superexchange-dominated ET reactions across oligo-*p*-phenylene bridges usually fall into the range of 0.4-0.8 Å^{-1}, depending on the dihedral angle between the adjacent aromatic rings.[78,79] At the same time, the distance attenuation parameter β^{TT} for the dyads was found to be 0.30 Å^{-1}, which is well within the ranges of values typically observed for TT energy transfer across conjugated bridges.[77,80-82] Thus, the experimental β^{ET} and β^{TT} in our systems are rather close to each other, $\beta^{TT}/\beta^{ET}=1.3$, i.e. significantly less 2.

From the mechanistic viewpoint, both ET and TT energy transfer in the dyads are likely to be mediated by through-bond couplings and occur *via* the superexchange mechanism, as opposed to incoherent hopping.[83] Indeed, for either electron, hole or triplet migration, the gaps between the initial states (PtP-Ph_n-^{S1}pRhB$^+$ for ET and HT; ^{T1}PtP-Ph_n-pRhB$^+$ for TT) and the hypothetic intermediate states involving the bridge (PtP$^{+\bullet}$-$Ph_n^{-\bullet}$-pRhB$^+$ for ET, PtP-$Ph_n^{+\bullet}$-pRhB$^{0\bullet}$ for HT and PtP-^{T1}Ph_n-pRhB) are positive and quite high (Fig. 7B), which is a condition required by the superexchange mechanism. It is the height of the tunneling barrier that determines the exponential distance attenuation factors in both ET and TT energy transfer process.[84,85] Estimations of the levels in Fig. 7B were based on our own electrochemical measurements and relevant literature data for oligophenylenes.[85,86] It was more appropriate in our case to consider HT (i.e. positive charge transfer from pRhB$^+$ to PtP) rather than ET, since the gap between the initial state and the hypothetically oxidized bridge ($Ph_n^{+\bullet}$) was lower than for the corresponding reduced bridge ($Ph_n^{-\bullet}$) (see SI, p.S12 for details).

Growing evidence suggests that for through-bond superexchange processes distance attenuation factors are not characteristics exclusively of the bridge, but rather depend on the combination of factors, including donor and acceptor and tunneling gap.[59,86,87] All three are almost always different for ET (or HT) and TT energy transfer processes. For example in our systems (Fig. 7B), the actual donor and acceptor states are PtP-Ph_n-^{S1}pRhB$^+$ for HT and ^{T1}PtP-Ph_n-pRhB$^+$ for TT, even though the individual chromophores and bridges are the same. Similarly, the bridge states are $Ph_n^{+\bullet}$ for HT and ^{T1} Ph_n for TT. Thus, valid comparison between distance attenuation factors should probably involve systems with energetically comparable initial, final and bridge states, rather than systems based on identical chromophores. In this regard, the ratio β^{TT}/β^{ET}=1.3 obtained for our dyads proves that ambiguity stemming from the use of different chromophores does not fully account for deviations from the theoretically predicted β^{TT}/β^{ET}=2 ratio.

Conclusions

We have demonstrated that in bichromophoric systems, consisting of phosphorescent triplet cores and auxiliary antenna dyes, emissive triplet states can be generated *via* electron transfer/radical recombination pathway, rather than directly as a result of the core-centered processes. The described PtP-pRhB$^+$ systems can serve as a prototype for future development of molecules, in which emission from triplet states is potentially susceptible to the control over the dynamics of intermediate radical pair states. Further optimization will need to focus on maximizing the efficiency of the ET/RP-ICS pathway relative to the direct charge recombination. As an extra benefit, the studied PtP-Ph_n-pRhB$^+$ dyads featured both ET and TT energy transfer processes in the same molecular systems, which allowed direct comparison between the corresponding distance attenuation factors β^{ET} and β^{TT}. Their ratio (β^{TT}/β^{ET}=1.3) was found to be much lower than theoretically predicted. Due to the flexibility in tuning the porphyrin redox potentials without altering its spectroscopic properties, PtP-based systems may instrumental in further studies of the relationship between ET and TT energy transfer processes.

Supplementary Material

Refer to Web version on PubMed Central for supplementary material.

Acknowledgments

Support of the grants from the National Institutes of Health of the USA (EB007279) and from the Research Foundation for Opto-Science and Technology (Hamamatsu, Japan) are gratefully acknowledged. Nanosecond transient absorption and fluorescence lifetime measurements were performed in the Regional Laser and Biomedical

Technology Laboratories (RLBL) (NIH/NCRR grant P41RR001348) with assistance of Dr. Thomas Troxler. Femtosecond transient absorption measurements were performed in the Ultrafast Laser Facility of the Photosynthetic Antenna Research Center (PARC), an Energy Frontier Research Center funded by the U.S. Department of Energy, Office of Science, Office of Basic Energy Sciences under Award Number DE-SC0001035. The authors are grateful to Professors Robin M. Hochstrasser (UPenn) and Dewey Holten (Washington University) for helpful discussions.

References

(1). Zhu TC, Finlay JC. Med. Phys. 2008; 35:3127. [PubMed: 18697538]

(2). Celli JP, Spring BQ, Rizvi I, Evans CL, Samkoe KS, Verma S, Pogue BW, Hasan T. Chem. Rev. 2010; 110:2795. [PubMed: 20353192]

(3). Singh-Rachford TN, Castellano FN. Coord. Chem. Rev. 2010; 254:2560.

(4). Ceroni P. Chem. Eur. J. 2011; 17:9560. [PubMed: 21717512]

(5). Sasabe H, Kido J. Chem. Mater. 2011; 23:621.

(6). Graham KR, Yang YX, Sommer JR, Shelton AH, Schanze KS, Xue JG, Reynolds JR. Chem. Mater. 2011; 23:5305.

(7). Wilson DF. Am. J. Physiol. Heart and Circ. Physiol. 2008; 294:H11. [PubMed: 17993593]

(8). Vinogradov, SA.; Wilson, DF. Porphyrin-dendrimers as biological oxygen sensors. In: Capagna, S.; Ceroni, P., editors. Designing Dendrimers. Wiley; New York: 2010.

(9). Rumsey WL, Vanderkooi JM, Wilson DF. Science. 1988; 241:1649. [PubMed: 3420417]

(10). Apreleva SV, Wilson DE, Vinogradov SA. Optics Letters. 2006; 31:1082. [PubMed: 16625910]

(11). Apreleva SV, Wilson DF, Vinogradov SA. Applied Optics. 2006; 45:8547. [PubMed: 17086268]

(12). Briñas RP, Troxler T, Hochstrasser RM, Vinogradov SA. J. Am. Chem. Soc. 2005; 127:11851. [PubMed: 16104764]

(13). Finikova OS, Troxler T, Senes A, DeGrado WF, Hochstrasser RM, Vinogradov SA. J. Phys. Chem. A. 2007; 111:6977. [PubMed: 17608457]

(14). Finikova OS, Lebedev AY, Aprelev A, Troxler T, Gao F, Garnacho C, Muro S, Hochstrasser RM, Vinogradov SA. ChemPhysChem. 2008; 9:1673. [PubMed: 18663708]

(15). Sakadzic S, Roussakis E, Yaseen MA, Mandeville ET, Srinivasan VJ, Arai K, Ruvinskaya S, Devor A, Lo EH, Vinogradov SA, Boas DA. Nat. Methods. 2010; 7:755. [PubMed: 20693997]

(16). Lećoq J, Parpaleix A, Roussakis E, Ducros M, Houssen YG, Vinogradov SA, Charpak S. Nat. Med. 2011; 17:893. [PubMed: 21642977]

(17). Steiner UE, Ulrich T. Chem. Rev. 1989; 89:51.

(18). Finikova OS, Chen P, Ou ZP, Kadish KM, Vinogradov SA. J. Photochem. Photobiol. A-Chem. 2008; 198:75. [PubMed: 19030124]

(19). Brocklehurst B. Chem. Soc. Rev. 2002; 31:301. [PubMed: 12357727]

(20). Hayashi, H. Introduction to Dynamic Spin Chemistry. Vol. 8. World Scientific; Singapore: 2004.

(21). Rodgers CT. Pure Appl Chem. 2009; 81:19.

(22). Wasielewski MR. J Org Chem. 2006; 71:5051. [PubMed: 16808492]

(23). Schulten K, Swenberg CE, Weller AZ. Phys. Chem.-Frankfurt. 1978; 111:1.

(24). Schulten K, Weller A. Biophys. J. 1978; 24:295. [PubMed: 309342]

(25). Ritz T, Adem S, Schulten K. Biophys. J. 2000; 78:707. [PubMed: 10653784]

(26). Rodgers CT, Hore PJ. PNAS. 2009; 106:353. [PubMed: 19129499]

(27). Kodis G, Liddell PA, Moore AL, Moore TA, Gust DJ. Phys. Org. Chem. 2004; 17:724.

(28). Maeda K, Henbest KB, Cintolesi F, Kuprov I, Rodgers CT, Liddell PA, Gust D, Timmel CR, Hore PJ. Nature. 2008; 453:387. [PubMed: 18449197]

(29). Ward HR. Acc. Chem. Res. 1972; 5:18.

(30). Lawler RG. Acc. Chem. Res. 1972; 5:25.

(31). Grissom CB. Chem. Rev. 1995; 95:3.

(32). Timmel CR, Henbest KB. Philos. Trans. A Math. Phys. Eng. Sci. 2004; 362:2573.

(33). Carbonera D. Photosynth. Res. 2009; 102:403. [PubMed: 19238576]

(34). Werner HJ, Schulten K, Weller A. Biochim. Biophys. Acta. 1978; 502:255. [PubMed: 306834]
(35). Levanon H, Norris JR. Chem. Rev. 1978; 78:185.
(36). Schulten K. Festkor.-Adv. Solid. St. 1982; 22:61.
(37). Schulten K, Weller A. Umschau. 1984; 84:779.
(38). Wiederrecht GP, Svec WA, Wasielewski MR, Galili T, Levanon H. J. Am. Chem. Soc. 2000; 122:9715.
(39). Kalyanasundaram, K. Photochemistry of Polypyridine and Porphyrin Complexes. Academic Press; London: 1992.
(40). Durr H, Bossmann S. Acc. Chem. Res. 2001; 34:905. [PubMed: 11714262]
(41). Montes VA, Pérez-Bolívar C, Agarwal N, Shinar J, Anzenbacher P. J. Am. Chem. Soc. 2006; 128:12436. [PubMed: 16984192]
(42). Montes VA, Pérez-Bolívar C, Estrada LA, Shinar J, Anzenbacher P. J. Am. Chem. Soc. 2007; 129:12598. [PubMed: 17902661]
(43). Tyson DS, Castellano FN. J. Phys. Chem. A. 1999; 103:10955.
(44). Harriman A, Hissler M, Khatyr A, Ziessel R. Chem. Commun. 1999; 735
(45). Ford WE, Rodgers MAJ. J. Phys. Chem. 1992; 96:2917.
(46). Whited MT, Djurovich PI, Roberts ST, Durrell AC, Schlenker CW, Bradforth SE, Thompson ME. J. Am. Chem. Soc. 2011; 133:88. [PubMed: 21142032]
(47). Kubin RF, Fletcher AN. J. Lumines. 1982; 27:455.
(48). Vinogradov SA, Wilson DF. Appl. Spectrosc. 2000; 54:849.
(49). Lindsey JS, Schreiman IC, Hsu HC, Kearney PC, Marguerettaz AM. J. Org. Chem. 1987; 52:827.
(50). Nguyen T, Francis MB. Org. Lett. 2003; 5:3245. [PubMed: 12943398]
(51). Araki N, Obata M, Ichimura A, Mikata Y, Yano S. Chem. Lett. 2004; 33:450.
(52). Wennerström O, Ericsson H, Raston I, Svensson S, Pimlott W. Tetrahedron Lett. 1989; 30:1129.
(53). Holmes AE, Das D, Canary JW. J. Am. Chem. Soc. 2007; 129:1506. [PubMed: 17243681]
(54). Senge MO. Acc. Chem. Res. 2005; 38:733. [PubMed: 16171316]
(55). Kim D, Holten D, Gouterman M, Buchler JW. J. Am. Chem. Soc. 1984; 106:4015.
(56). Eastwood D, Gouterman M. J. Mol. Spectrosc. 1970; 35:359.
(57). Ou ZP, Chen P, Kadish KM. Dalton Trans. 2010; 39:11272. [PubMed: 20976327]
(58). Rehm D, Weller A. Israel J. Chem. 1970; 8:259.
(59). Wenger OS. Chem. Soc. Rev. 2011; 40:3538. [PubMed: 21512684]
(60). Miyaura N, Suzuki A. Chem. Rev. 1995; 95:2457.
(61). Kobayashi T, Straub KD, Rentzepis PM. Photochem. Photobiol. 1979; 29:925.
(62). Ponterini G, Serpone N, Bergkamp MA, Netzel TL. J. Am. Chem. Soc. 1983; 105:4639.
(63). Korobov VE, Shubin VV, Chibisov AK. Chem. Phys. Lett. 1977; 45:498.
(64). Saik VO, Goun AA, Fayer MD. J. Chem. Phys. 2004; 120:9601. [PubMed: 15267972]
(65). Okada T, Mataga N, Sakata Y, Misumi S. J. Photochem. 1981; 17:130.
(66). Dance ZE, Mi Q, McCamant DW, Ahrens MJ, Ratner MA, Wasielewski MR. J. Phys. Chem. B. 2006; 110:25163. [PubMed: 17165960]
(67). Livesey AK, Brochon JC. Biophys. J. 1987; 52:693. [PubMed: 19431708]
(68). Pevenage D, Van der Auweraer M, De Schryver FC. Chem. Phys. Lett. 2000; 319:512.
(69). Korobov VE, Chibisov AK. Usp. Khim.(russ). 1983; 52:43.
(70). Kunavin NI, Nurmukhametov RN, Khachaturova GT. J. Appl. Spectrosc. 1977; 26:735.
(71). Chambers RW, Kearns DR. J. Phys. Chem. 1968; 72:4718.
(72). Morales AF, Accorsi G, Armaroli N, Barigelletti F, Pope SJA, Ward MD. Inorg. Chem. 2002; 41:6711. [PubMed: 12470066]
(73). Lavie-Cambot A, Lincheneau C, Cantuel M, Leydet Y, McClenaghan ND. Chem. Soc. Rev. 2010; 39:506. [PubMed: 20111775]
(74). Chambers RW, Kearns DR. Photochem. Photobiol. 1969; 10:215. [PubMed: 5824756]
(75). Closs GL, Piotrowiak P, Macinnis JM, Fleming GR. J. Am. Chem. Soc. 1988; 110:2652.

(76). Closs GL, Johnson MD, Miller JR, Piotrowiak P. J. Am. Chem. Soc. 1989; 111:3751.
(77). Welter S, Salluce N, Belser P, Groeneveld M, De Cola L. Coord. Chem. Rev. 2005; 249:1360.
(78). Helms A, Heiler D, McLendon G. J. Am. Chem. Soc. 1992; 114:6227.
(79). Wenger OS, Leigh BS, Villahermosa RM, Gray HB, Winkler JR. Science. 2005; 307:99. [PubMed: 15637275]
(80). Andreasson J, Kajanus J, Martensson J, Albinsson B. J. Am. Chem. Soc. 2000; 122:9844.
(81). Vura-Weis J, Abdelwahed SH, Shukla R, Rathore R, Ratner MA, Wasielewski MR. Science. 2010; 328:1547. [PubMed: 20558715]
(82). Barigelletti F, Flamigni L, Guardigli M, Juris A, Beley M, Chodorowski-Kimmes S, Collin JP, Sauvage JP. Inorg. Chem. 1996; 35:136. [PubMed: 11666175]
(83). May, V.; Kühn, O. Charge and Energy Transfer Dynamics in Molecular Systems. Third, Revised and Enlarged ed. Wiley-VCH; Weinheim: 2011.
(84). Gray HB, Winkler JR. PNAS. 2005; 102:3534. [PubMed: 15738403]
(85). Wenger OS. Acc. Chem. Res. 2011; 44:25. [PubMed: 20945886]
(86). Albinsson B, Eng MP, Pettersson K, Winters MU. Phys. Chem. Chem. Phys. 2007; 9:5847. [PubMed: 17989792]
(87). Eng MP, Albinsson B. Chem. Phys. 2009; 357:132.

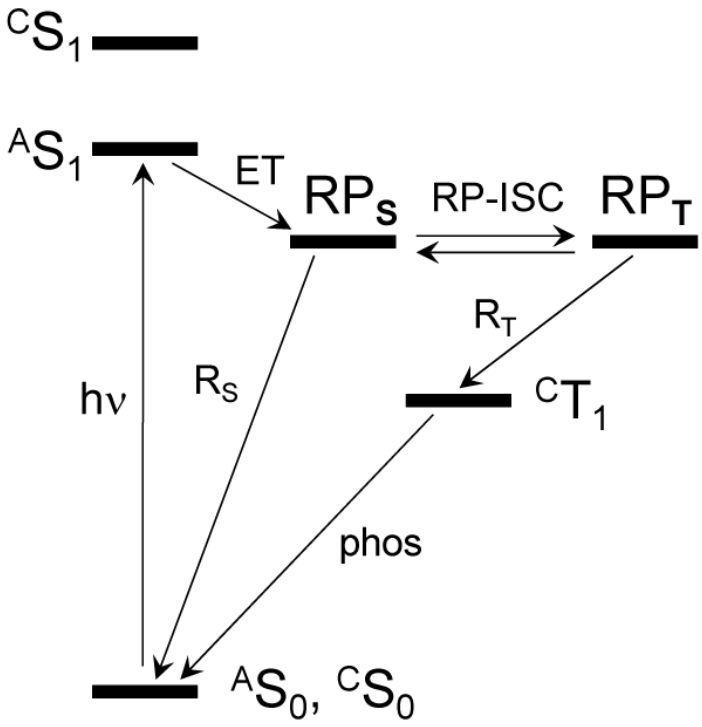

Figure 1.
Energy diagram of bichromophoric antenna (A) – core (C) systems, in which the local triplet state of the core ($^{C}T_1$) is populated *via* excitation of the antenna, electron transfer (ET) with formation of the singlet radical pair (RP_S), intersystem crossing (RP-ISC) and radical recombination (R_T) from the resulting triplet radical pair (RP_T). Alternatively, RP_S undergoes charge recombination R_S, yielding the ground state species.

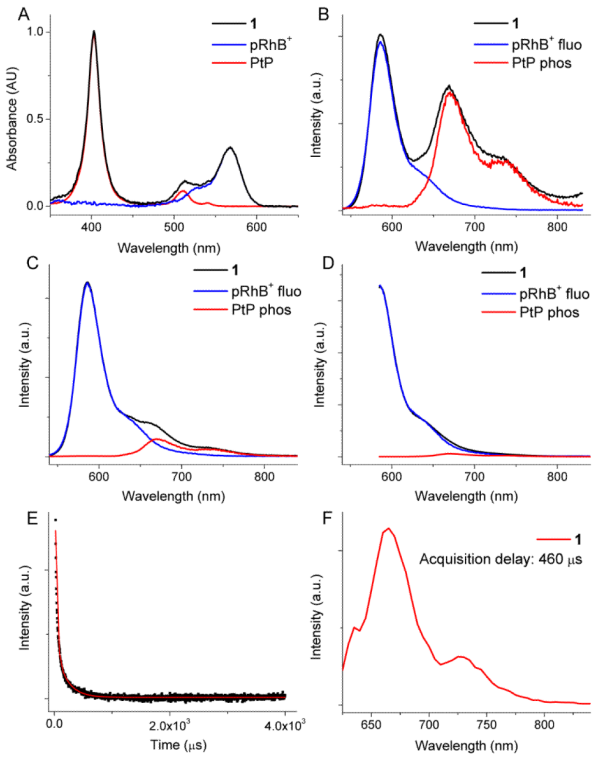

Figure 2.

(A) Normalized absorption spectra of PtP, $pRhB^+$ and dyad **1** in benzonitrile. Emission spectra of **1** acquired using different excitation wavelengths (λ_{ex}): 425 nm (B), 510 nm (C), and 580 nm (D). The spectra of the components were obtained by linear decomposition. Phosphorescence decay (E) and phosphorescence spectrum registered with delay of 460 μs (F) upon pulsed excitation at 580 nm.

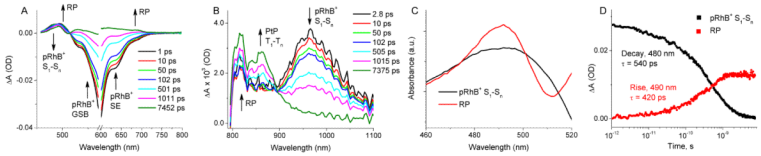

Figure 3.

(A) FSTA spectra of **1** in the visible range at selected times after excitation by a femtosecond laser pulse: FWHM 90 fs, λ_{max}=580 nm. (B) FSTA spectra of **1** in the near infrared (NIR) range. (C) Decay-associated spectra obtained by global fitting of the transients shown in A. (D) Evolution of the spectra shown in C at selected wavelengths (480 and 490 nm) and the corresponding time constants obtained by single-exponential fitting. GSB – ground state bleaching. SE – stimulated emission.

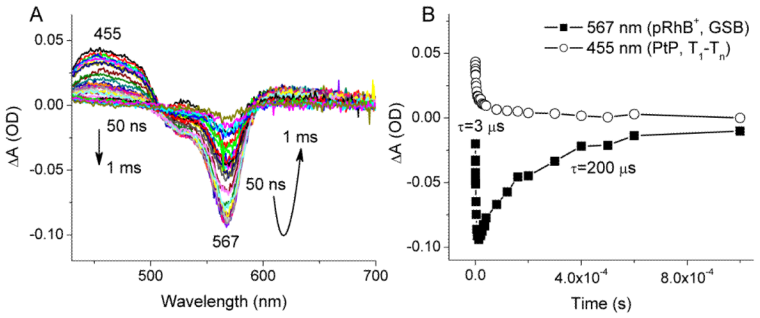

Figure 4.

(A) Nanosecond transient absorption spectra of dyad **1** (λ_{ex}=532 nm, pulse FWHM 10 ns). (B) Changes in the absorbance at 567 nm – ground state bleaching (GSB) of $pRhB^+$, and 455 nm – $T_1 \rightarrow T_n$ absorption of PtP.

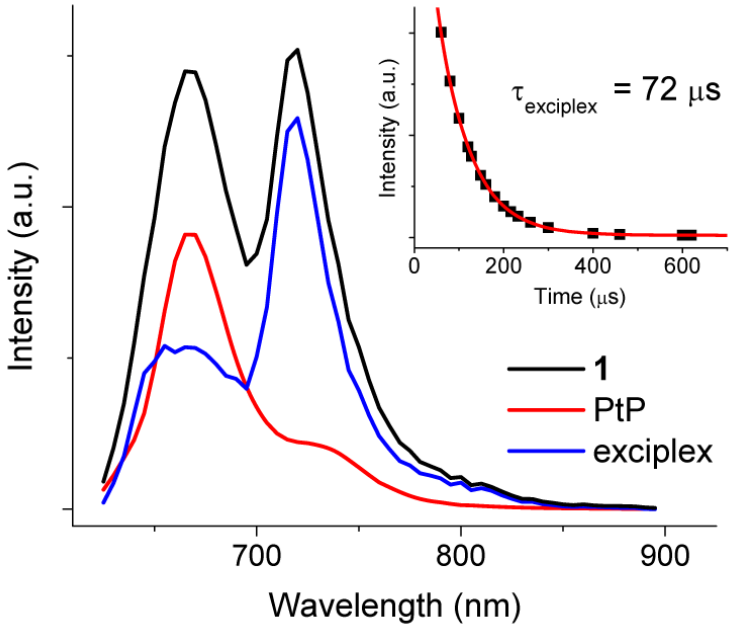

Figure 5.
Emission spectra of **1** at 60 μs after excitation pulse (λ_{max}=580 nm). Inset: decay of the emission line at 720 nm.

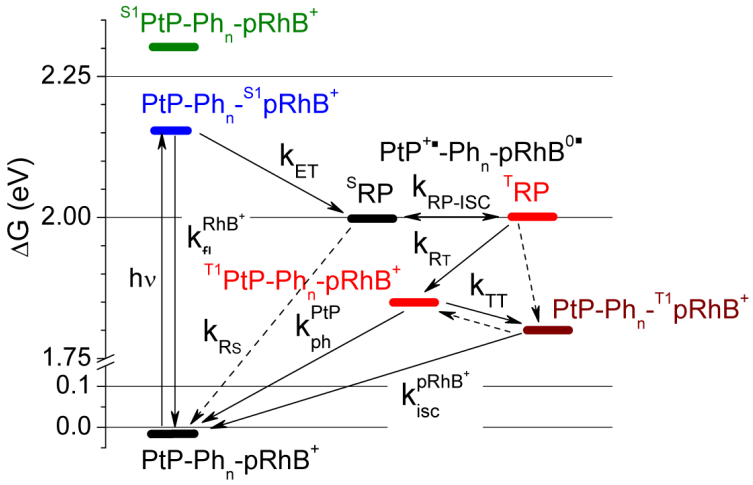

Figure 6.

Pathways occurring in PtP-RhB dyads. The arrows indicate processes whose rate constants were deduced from the spectroscopic measurements. Dashed lines indicate routes for which the rate constants were not experimentally obtained. k_{RS} and k_{RT} refer to the recombination of the singlet and triplet radical pairs, respectively. k_{TT} – rate constant for the forward TT energy transfer.

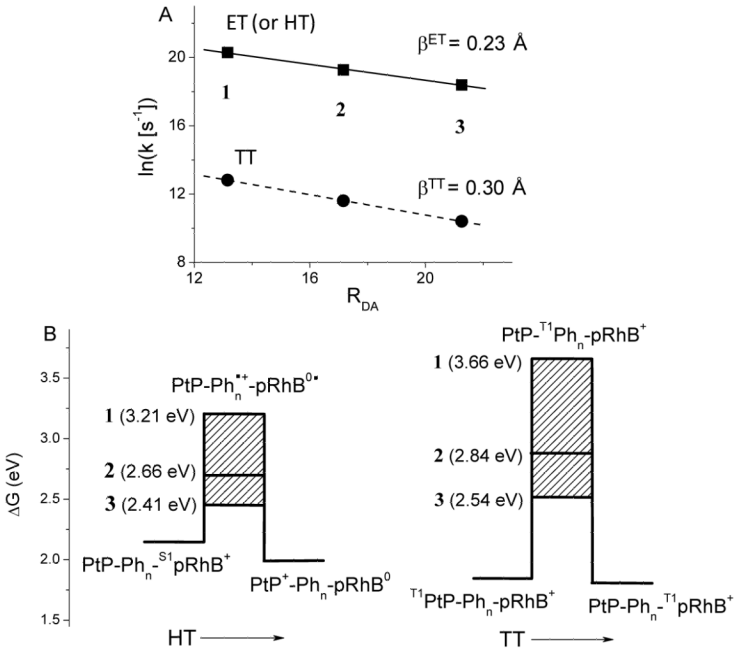

Figure 7.

A) Distance dependencies of the rate constants for the primary ET, or HT, (□, k_{ET}, PtP→pRhB$^+$) and TT energy transfer (•, k_{TT}, PtP→pRhB$^+$). B) Energy diagrams for HT (hole transfer) and TT energy transfer in the dyads, showing relative heights of the tunneling barriers.

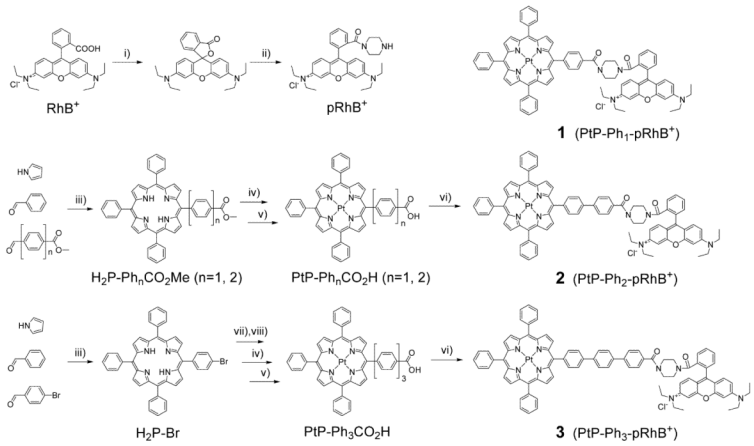

i) NaOH/EtOAc; ii) $AlMe_3$/piperazine; iii) a) $BF_3{\cdot}Et_2O/CH_2Cl_2$; b) DDQ; iv) $PtCl_2$/PhCN; v) KOH/THF; vi) HBTU/DIPEA/DMF; vii) $B_2pin_2/PdCl_2(dppf)$/DMF; viii) 4-bromo-4'-methoxycarbonyl-biphenyl/$Pd(PPh_3)_4$/KOAc/DMF.

Scheme 1.
Synthesis of dyads **1**-**3**.

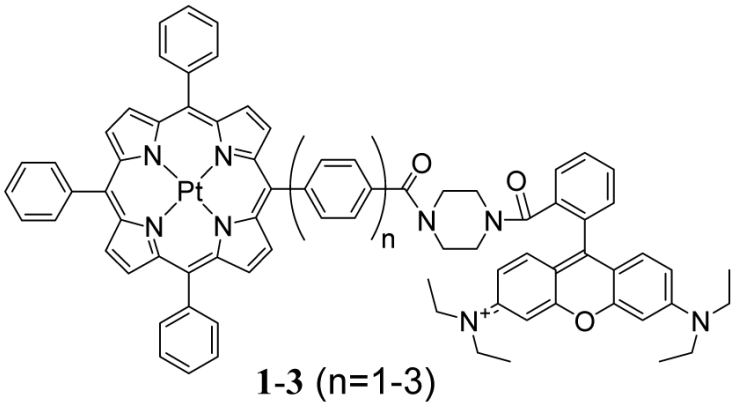

Chart 1.
Studied dyads **1**-**3**.

Table 1

Selected photophysical properties of the PtP-Ph_n-$pRhB^+$ dyads **1-3** (n=1-3) and of their components.[a] Porphyrins PtP-Ph_nCO_2H (Scheme 1) are abbreviated in the Table as PtP_n, for n=1-3.

	λ_{abs} (nm)	λ_{em} (nm) (em. type)[b]	Φ_{fl}[c] λ_{ex} (510 nm)	τ_{fl} (ns)[d]	Φ_{ph}[c,e] λ_{ex} (425 nm)	Φ_{ph}[c,f] λ_{ex} (580 nm)	τ_{ph}(μs)[g]
1	408, 517, 567	585 (f), 670 (p), 730 (p)	0.17 ± 0.04	1.0	0.020 ± 0.02	0.005 ± 0.001	3,[h] 200
2	408, 517, 567	585 (f), 670 (p), 730 (p)	0.24 ± 0.03	1.7	0.031 ± 0.05	0.010 ± 0.002	10,[h] 170
3	407, 516, 567	585 (f), 670 (p), 730 (p)	0.38 ± 0.03	2.2	0.040 ± 0.06	0.010 ± 0.001	30
$pRhB^+$	567	585 (f)	0.45 ± 0.03	2.8	--		--
PtTPP	407, 514, 542	670 (p), 735 (p)	--	--	0.13 ± 0.01[j]		53 ± 1
PtP_1	406, 512, 543	670 (p), 735 (p)	--	--	0.08 ± 0.01[j]		43 ± 1
PtP_2	407, 512, 544	670 (p), 735 (p)	--	--	0.07 ± 0.01[j]		35 ± 1
PtP_3	406, 512, 541	670 (p), 735 (p)	--	--	0.05 ± 0.01[j]		34 ± 1

[a] All measurements were performed in deoxygenated anhydrous benzonitrile.

[b] f – fluorescence, p – phosphorescence.

[c] Emission quantum yields were determined relative to the fluorescence of Rhodamine 6G in EtOH (Φ_{fl}=0.95).[47]

[d] λ_{ex}=405 nm.

[e] Corresponds to the phosphorescence emitted as a result of direct excitation of PtP (Soret band), followed by intrachromophoric ISC.

[f] Phosphorescence emitted as a result of the pathway involving ET and RP-ISC.

[g] λ_{ex}=510 nm.

[h] Distributions of lifetimes (see text for details).

[j] λ_{ex} = 510 nm.

Table 2

Rate constants associated with the pathways displayed in Fig. 6.[a]

	k_{fl} $\times 10^8$ s^{-1}	k_{ET} $\times 10^8$ s^{-1}	k_{RT} $\times 10^9$ s^{-1}	k_{TT} [b] $\times 10^5$ s^{-1}	k_{ph}^{PtP} [c] $\times 10^5$ s^{-1}	k_{isc}^{pRhB+} $\times 10^3$ s^{-1}
1	10.0	6.7	2.4	3.4	3.3, 0.05	5.0
2	5.9	2.3	1.2	1.1	1.0, 0.06	6.7
3	4.5	0.97	-	0.33	0.33	~5.0

[a] All rate constants correspond to the measurements performed in deoxygenated benzonitrile solutions at room temperature.

[b] Obtained from NSTA data.

[c] Peak maxima in the lifetime distributions.